

Electronic Supplementary Information

Location-Specific Nanoplasmonic Sensing of Biomolecular Binding to Lipid Membranes with Negative Curvature

Juliane Junesch,^a Gustav Emilsson,^{a†} Kunli Xiong,^{a†} Shailabh Kumar,^b Takumi Sannomiya,^c Hudson Pace,^a Janos Vörös,^d Sang-Hyun Oh,^b Marta Bally^a and Andreas B. Dahlin.^{a*}

^a Dept. of Applied Physics, Chalmers University of Technology, 41296 Göteborg, Sweden.

^b Dept. of Electrical and Computer Engineering, University of Minnesota, 55455 Minneapolis, USA.

^c Dept. of Innovative and Engineered Materials, Tokyo Institute of Technology, 152-8550 Tokyo, Japan.

^d Dept. of Information Technology and Electrical Engineering, Swiss Federal Institute of Technology, 8092 Zürich, Switzerland.

† These authors contributed equally and substantially.

* Corresponding author: adahlin@chalmers.se

Additional sensing results

The spectral shifts in peak and dip were monitored also during surface functionalization of SiO₂ coated nanowells, that is for bilayer formation with vesicles and during adsorption of a copolymer consisting of 50% biotinylated poly(ethylene glycol) grafted to a poly(L-lysine) backbone. The kinetics of vesicle adsorption (Fig. 1) are especially important to monitor since they provide an additional verification of bilayer formation.[1] This is because as the vesicles rupture and fuse into a bilayer, high refractive index material is moved closer to the surface, where the confined electromagnetic field is higher.[2] This leads to an additional signal which makes the overall kinetics deviate from a typical “Langmuir-shaped” curve (signal proportional to $(1 - \exp(-t/\tau))$ where τ is the characteristic time for binding). Instead, the kinetics should appear more linear, which is in agreement with the data in Fig. 1. For comparison, it can be seen that the copolymer adsorption generates binding kinetics with much higher curvature (Fig. 2).

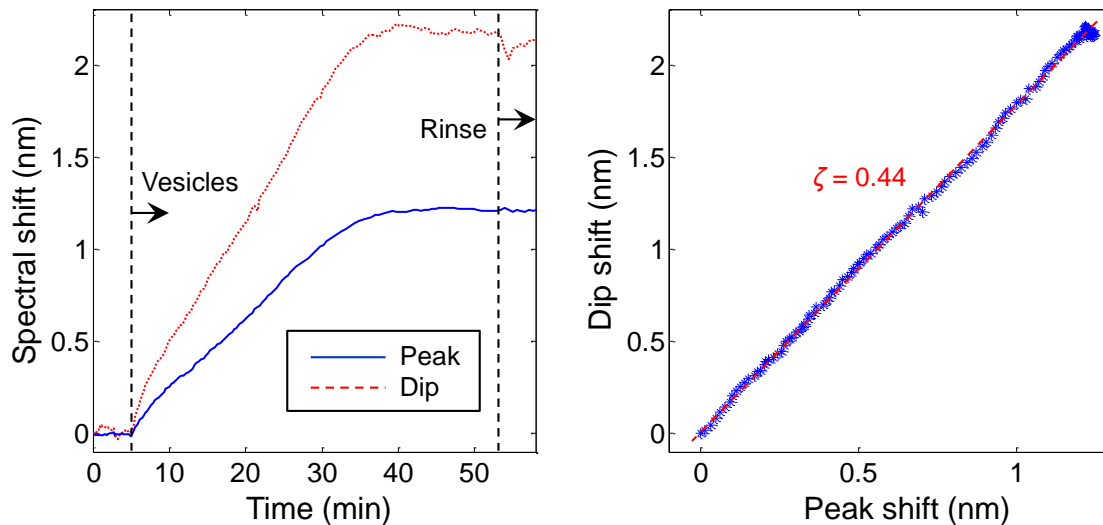


Fig. 1 Bilayer formation by vesicle adsorption and rupturing. The left plot shows the shifts in extinction peak and dip. A scatter plot is shown to the right. A vesicle concentration of 100 $\mu\text{g/ml}$ was introduced to the SiO₂ coated nanowells.

Both bilayer formation and polymer adsorption gave approximately the same value of ζ (0.4-0.5) as expected when adsorption occurs on the same SiO₂ coating everywhere in the structure. Also, the copolymer forms a layer which has a thickness that is similar to a lipid bilayer (~5 nm) since the poly(ethylene glycol) blocks are highly flexible with a molecular weight of only 2 kDa (3.4 kDa for the biotinylated branches). The differences in absolute signals when comparing Fig. 1 with Fig. 2 are due to the higher refractive index change for a lipid bilayer in comparison with the highly hydrated copolymer. For bilayer formation, ζ is constant throughout the bilayer formation process (scatter plot in Fig. 1). The data of copolymer adsorption has higher uncertainty due to slower binding and lower signals but clearly has approximately the same ζ (line drawn in Fig. 2), showing that the copolymer brush coats also the inside of the nanowells.

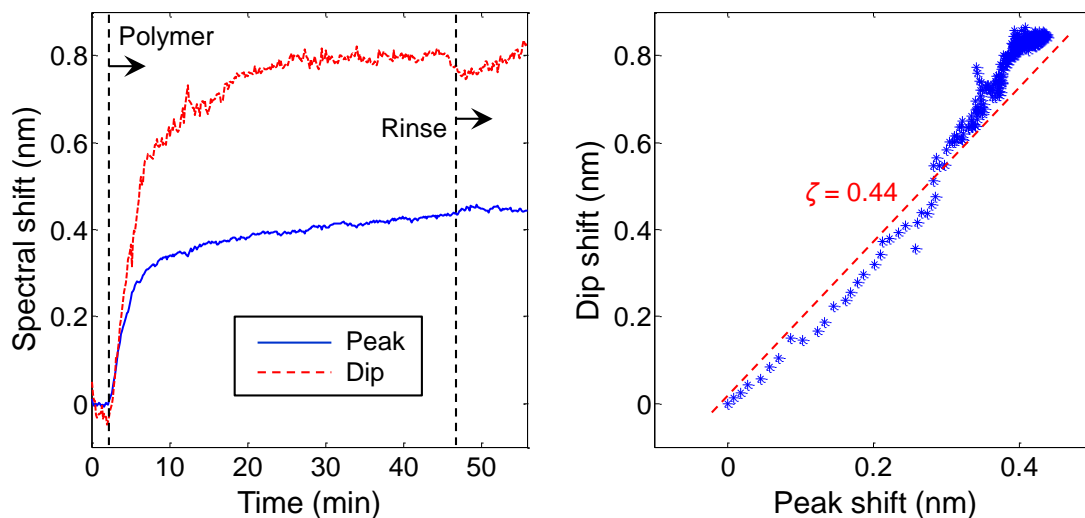


Fig. 2 Adsorption of biotinylated copolymer on SiO₂ coated nanowells. The left plot shows the shifts in extinction peak and dip. A scatter plot is shown to the right. A copolymer concentration of 20 $\mu\text{g/ml}$ was introduced.

Numerical simulations of location-specific detection

To verify that the location-specific sensitive detection obeys electromagnetic theory we conducted numerical simulations in COMSOL Multiphysics. The simulated extinction spectrum is shown in Fig. 3. As in previous work,[3, 4] the nanowell pattern was represented by a long-range ordered array, here by square periodicity of 230 nm. This is approximately the characteristic spacing between the nanowells, which is determined by the colloids used in the lithography and hence represents the short-range ordered pattern well. The simulated nanowell geometry (main text) was carefully selected from representative images of nanowells (Fig. 7). The refractive index values were set to 2.1 for Nb₂O₅, 1.52 for glass and 1.33 for water. The permittivity of Au was taken from Johnson & Christy.[6] Overall we find the spectrum in Fig. 3 in agreement with the experimental spectrum (main text). The main difference is the sharper resonance features which can be expected when simulating an idealized structure.

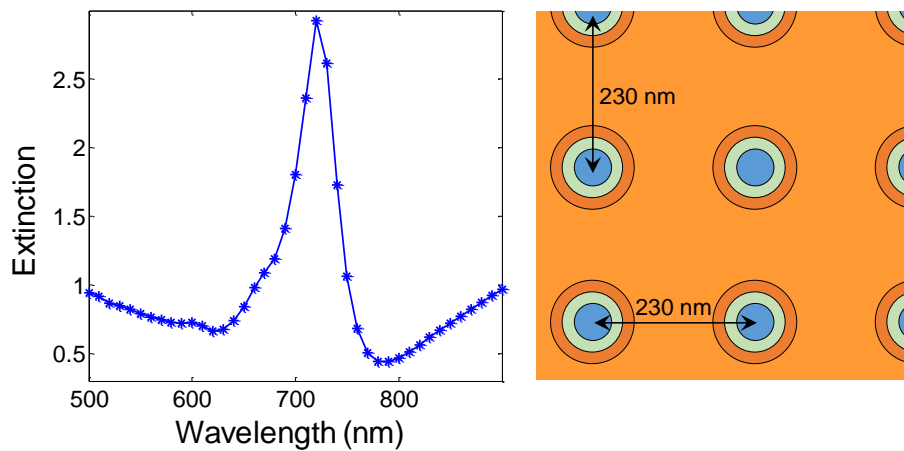


Fig. 3 Simulated extinction spectrum of nanowells in water (COMSOL Multiphysics). An infinite long-range ordered array (here square arrangement) was used to represent the experimental structures which are short-range ordered. The simulated nanowell dimensions were exactly those determined from imaging of nanowells.

To simulate the spectral shifts upon molecular binding we introduced a coating that was 5 nm thick and had a refractive index of 1.5. (These values are comparable to the real thickness and refractive index values of OEG monolayers and dense protein films.) Finely discretized wavelength intervals around the peak and dip positions were analyzed to determine the shifts (error ± 0.1 nm). The coating was placed on different regions in the nanostructure (Fig. 4). Overall the spectral shifts were comparable to those experimentally measured and the increased value of ζ inside the nanowells due to a strongly reduced peak shift was confirmed. Note in particular that for “binding” only inside the nanowells the simulations reproduced the very low peak shift (< 0.1 nm experimentally and in simulations).

Quantitatively, the simulation results on resonance shifts were dependent on the exact shape of the nanowells. For instance, making the Au top aperture wall vertical or making the glass bottom tens of nm wider changed the shifts in peak and dip. However, a clear qualitative trend of increased ζ inside the nanowells compared to on the planar surface was observed in all simulations. We also analyzed the shifts in peak and dip using the multiple multipole program.[5] A “molecule” with diameter 16 nm and refractive index of 3 was placed on different locations, either above the Au surface or along the nanowell with a distance of 4 nm from the surface. These simulations were performed on a simplified nanowell geometry with vertical walls, in contrast to the COMSOL simulations in which the geometry was much closer to the real nanowells. Also, a single molecule which is larger and with higher refractive index than the actual molecular layers is introduced. Thus, these results were considered less accurate in principle, but did reproduce the tendency of increased ζ down inside a nanowell compared to the planar surface (not shown).

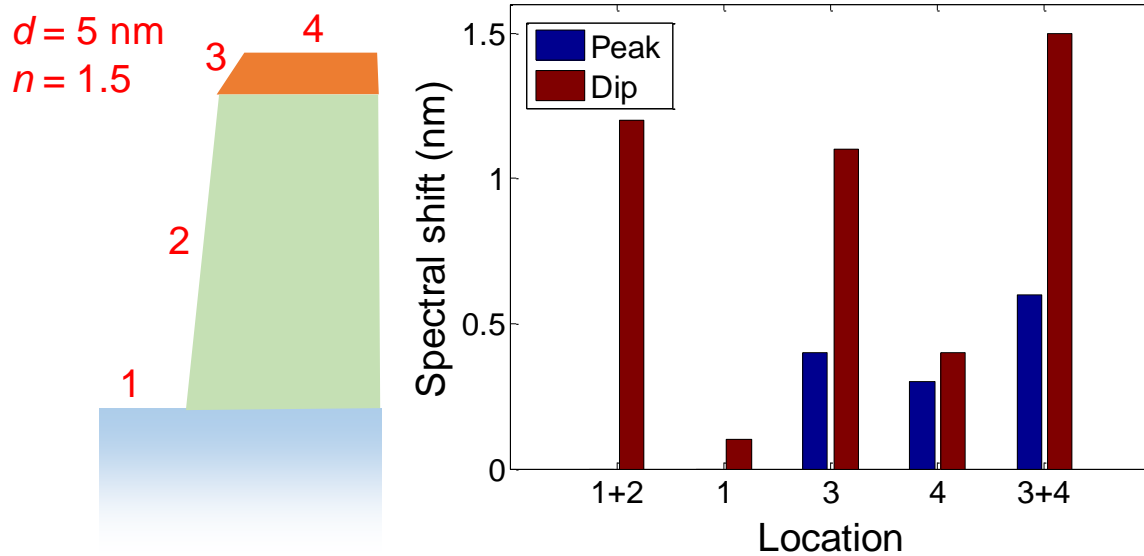


Fig. 4. Simulated peak and dip shift upon molecular binding inside the nanowells by COMSOL Multiphysics. A layer with thickness 5 nm and refractive index 1.5 is introduced on one or more locations: 1 (glass bottom), 2 (Nb₂O₅ wall), 3 (Au wall) or 4 (top Au surface).

The basic model used in COMSOL was 3D Electromagnetic Waves, Frequency Domain. The structure included two perfectly matched layers (PML) on the top and bottom, which were used to absorb reflected, transmitted and scattered light. Under the top PML layer an import layer was placed, which set the incident light and the environment of the samples. The sample layer with the nanostructure was below the import layer and the glass substrate layer was below the sample layer. The first calculation step was for the background field and the second step was for the field distribution after inserting the nanostructure. (The reason is that the import layer cannot produce an incident wave when it is directly connected with PML layer, so we could not use the top PML layer in the first calculation step.)

Quartz crystal microbalance data

It is well-known that a dense monolayer with OEG chains can make gold inert to protein adsorption and that this can be achieved without influencing surrounding oxide materials.[7] Still, in order to further verify that protein adsorption can occur specifically inside the nanowells, we performed quartz crystal microbalance with dissipation monitoring (QCM-D) experiments on four different sensor crystals: Au passivated with OEG, clean Au, Nb₂O₅ and borosilicate. Results are shown in Fig. 5. At 5 min 100 µg/mL of NeutrAvidin is introduced, which leads to adsorption on all surfaces except the modified Au which shows no detectable binding. The system is rinsed at 25 min which appears to result in a small amount of protein desorption on borosilicate and Nb₂O₅, but the proteins are generally irreversibly bound. We have also used QCM-D to verify that the thiolated OEG only binds to Au and not Nb₂O₅ or glass as expected (data not shown).

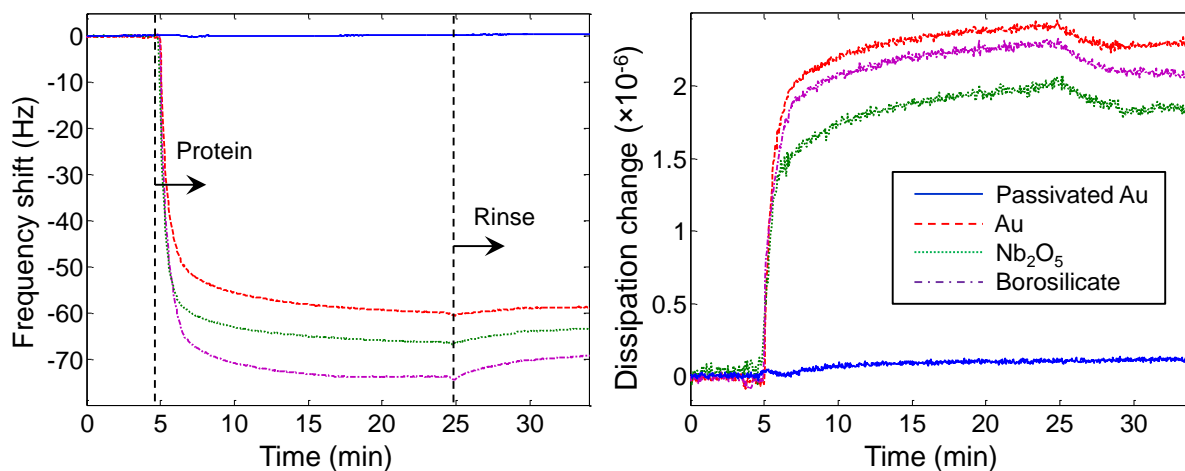


Fig. 5 Verification of surface chemistry by quartz crystal microbalance with dissipation monitoring using different sensor coatings. The frequency shifts are shown in the left plot and the simultaneous dissipation changes to the right. The concentration protein introduced was 100 µg/ml.

QCM-D crystals with Au or borosilicate (Biolin Scientific) were cleaned with UV O₃ before experiments. For analyzing Nb₂O₅ surfaces, 200 nm Nb₂O₅ was sputter coated on Au crystals using the same protocol as when fabricating nanowells. Crystals with borosilicate coating were purchased from the manufacturer. Data is shown for the third overtone. The experimental variation in frequency shifts for adsorption of avidin on Nb₂O₅ and borosilicate was ± 10 Hz when cleaning and reusing sensor crystals.

Fluorescence recovery after photobleaching

In order to further characterize the lipid membranes we measured the fluorescence recovery after photobleaching spots on a membrane formed with vesicles containing a small fraction of a fluorescent lipid. Example data is shown in Fig. 6 for a ~ 100 μm spot with $t = 0$ set just after the bleaching event. The diffusion constant can be roughly estimated from the characteristic recovery time of $\tau \approx 300$ s and the diffused distance of $R \approx 50$ μm as $D = R^2/(4\tau)$. This gives D equal to a few $\mu\text{m}^2/\text{s}$ which is very similar to values previously determined[1] (~ 2 $\mu\text{m}^2/\text{s}$).

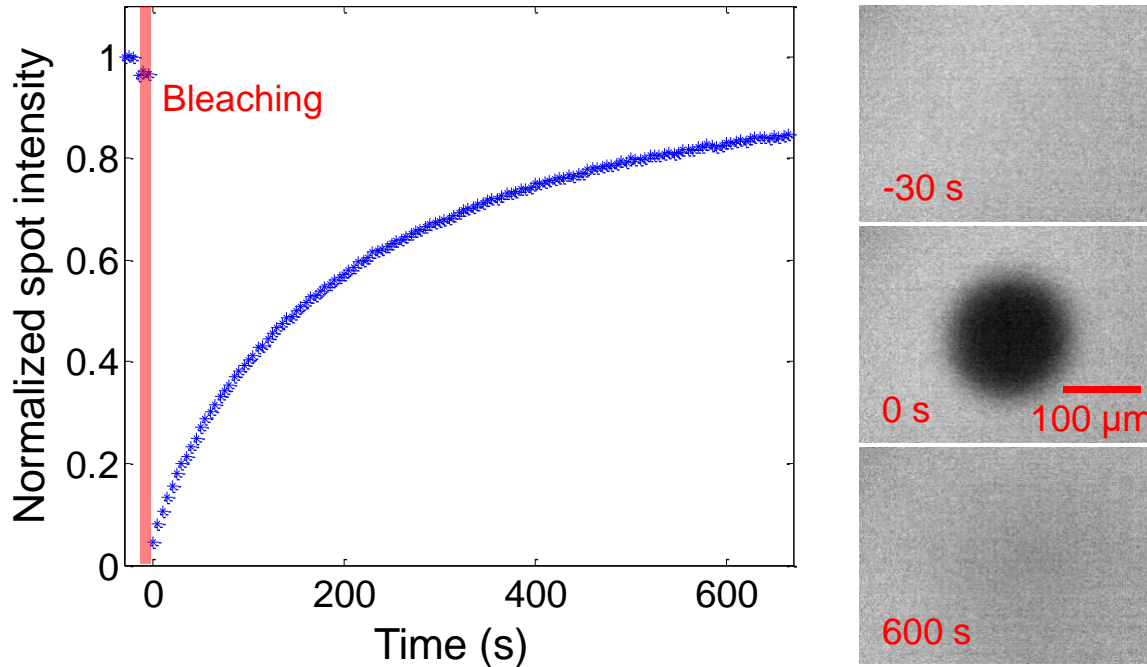


Fig. 6 Fluorescence recovery after photobleaching on a nanowell sample with a membrane containing a small fraction fluorescent lipids. The intensity of the bleached spot is shown as a function of time after bleaching. Fluorescence images of the spot are shown to the right.

The measurements were performed with a Nikon Eclipse TE2000U microscope (Nikon Corporation) with a 20× objective (Nikon) and a TRITC filter cube. Bleaching was done with a Kr-Ar mixed gas ion laser, 530.9 nm wavelength, while the recovery was monitored with a cooled CCD-camera (iXon DV887-BI, Andor Technology) under illumination with a super high pressure mercury lamp. The images were collected every 5 seconds. To compensate for uneven illumination and detector dark count, pre-bleach images as well as images without illumination were also acquired. Data was normalized by taking the difference between intensity of bleached spot at current time and intensity immediately after photobleaching, divided by the difference between intensity of the spot before photobleaching and intensity immediately after photobleaching.

Additional electron microscopy images

Fig. 7 shows two additional images of nanowells, before and after SiO₂ coating. The purpose is to show the arrangement of nanowells over a larger area and to show that the bottom is smaller than the top aperture. We estimated the diameter at the bottom of the nanowells to be down to 50 nm and the top apertures up to 150 nm. Further, the Au walls appeared not vertical and judging from close inspection of the images it seems likely that some Au also covers the Nb₂O₅ walls. Movement of material can be expected during directional plasma etching with high power (here 150 W) since such processes have both chemical “etching” and physical “milling” components. Indeed, the initial apertures in the Au film should be 100 nm like the colloidal particles used for the lithography. It seems plausible that material from the etched Au edges ends up on the Nb₂O₅ as the adhesion between the materials is good. (Such fine structural details were unfortunately too complicated to implement in the numerical simulations.) We noted that the exact shape of the nanowells is sensitive to the process parameters (especially the dry etching) which needs to be controlled as precisely as possible. Small changes in the shape of the nanowells were found to influence the final spatial sensing results. For instance, if a lower power is used for etching, the top Au apertures and the Nb₂O₅ walls assume a different shape and the signals in peak and dip change are modified. However, qualitatively the spatial sensing result was always clearly observed, i.e. ζ always strongly increased for binding inside the nanowells compared with the planar surface (which was also the case in all simulations).

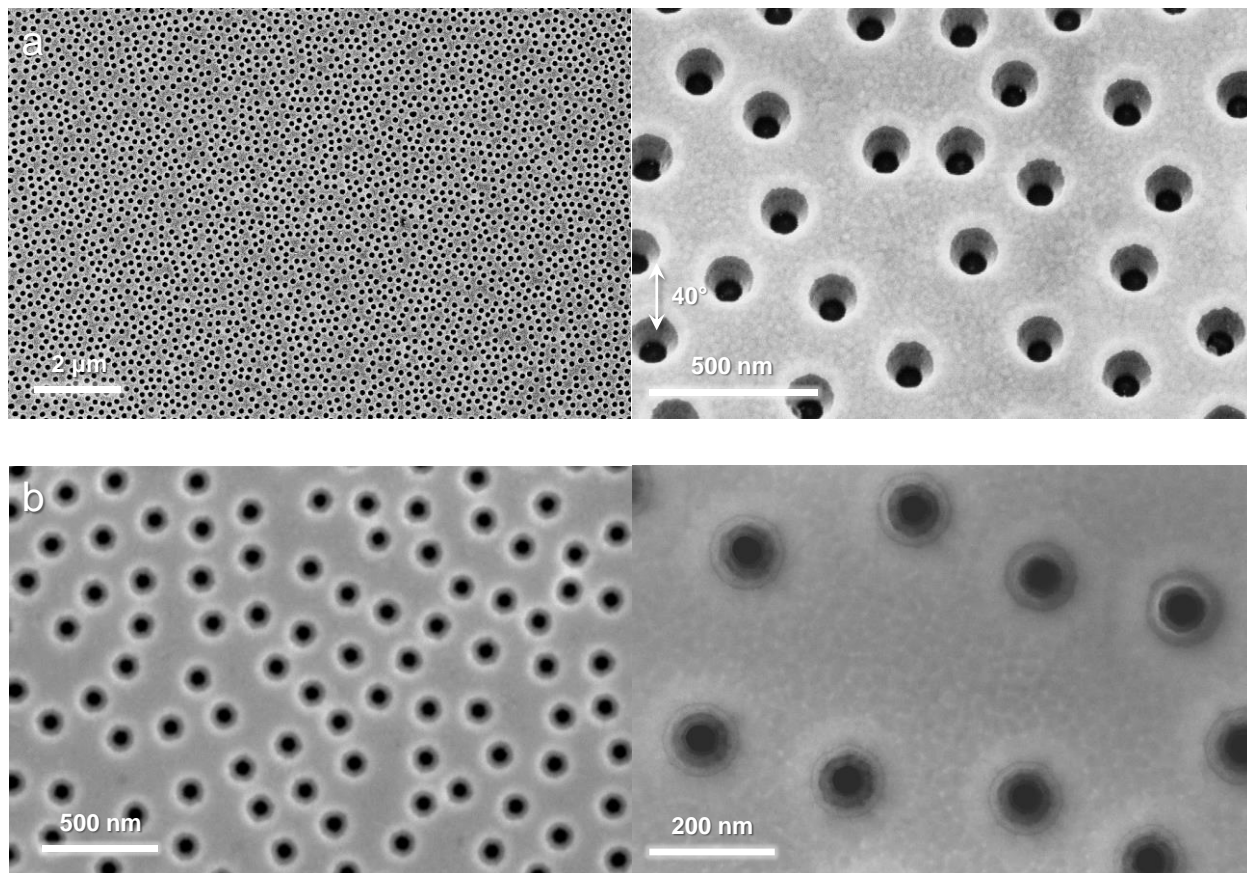


Fig 7 Large area images of nanowells before (a) and after (b) SiO₂ coating. A close up is shown for both cases, illustrating the shape of the nanowells. In (a) tilt is used and in (b) the material contrast can be used to estimate the critical dimensions.

Nanowells were also imaged by scanning electron microscopy after sensing experiments. We emphasize that when performing this kind post-binding imaging one cannot exclude possible effects from drying the sample and exposing it to vacuum. (A point which appears to be rarely discussed in the literature for this kind of experiments.) The images are thus presented as supportive rather than definite proof of accumulation inside nanowells. All samples were, however, cleaned before the binding experiments and never exposed to other colloidal particles of any kind, so the observed objects should definitely be VLPs (Fig. 8) and avidin-covered colloids

(Fig. 9) respectively. Further, the VLPs were destroyed by the electron beam during imaging, as expected for organic material, while the colloids showed no tendency of being destroyed, confirming that they were inorganic.

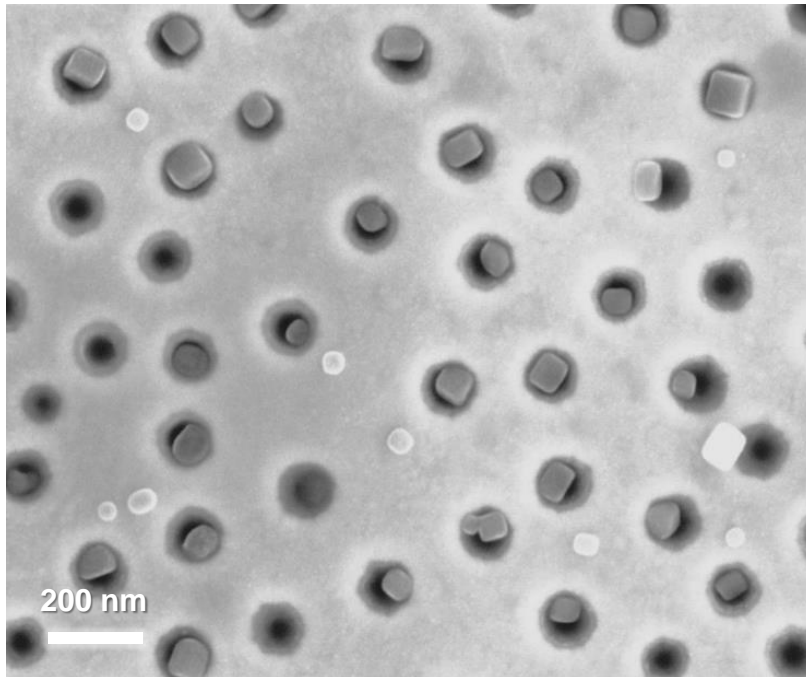


Fig. 8 A nanowell sample after binding of VLPs to a membrane with glycosphingolipids.

Fig. 8 shows an image of a sample post VLP binding. Relatively few VLPs were found on the planar surface and most were located inside nanowells. The enlarged and elongated VLPs can be explained by fusion of multiple VLPs, as it is well-known that the norovirus capsid assembly is a dynamic equilibrium sensitive to environmental changes. However, we cannot deduce when fusion of VLPs would occur. (It could occur at some point while preparing the sample for electron microscopy imaging or perhaps even during the binding experiments.) Nevertheless, we consider the observation of enlarged viral capsids preferentially located inside nanowells relevant.

As shown in Fig. 9, silica colloids could be visualized inside nanowells after a short time (~1 min) of binding to a membrane containing biotinylated lipids. No colloids were observed on the planar surface. Based on the size of the SiO₂ coated nanowells and the avidin-coated colloids one should not expect multiple colloids next to each other. Those observed in Fig. 9 are likely stacked on top of each other to some extent in the >200 nm deep wells. We cannot exclude that there are more colloids further down in the well that are not visible in the images.

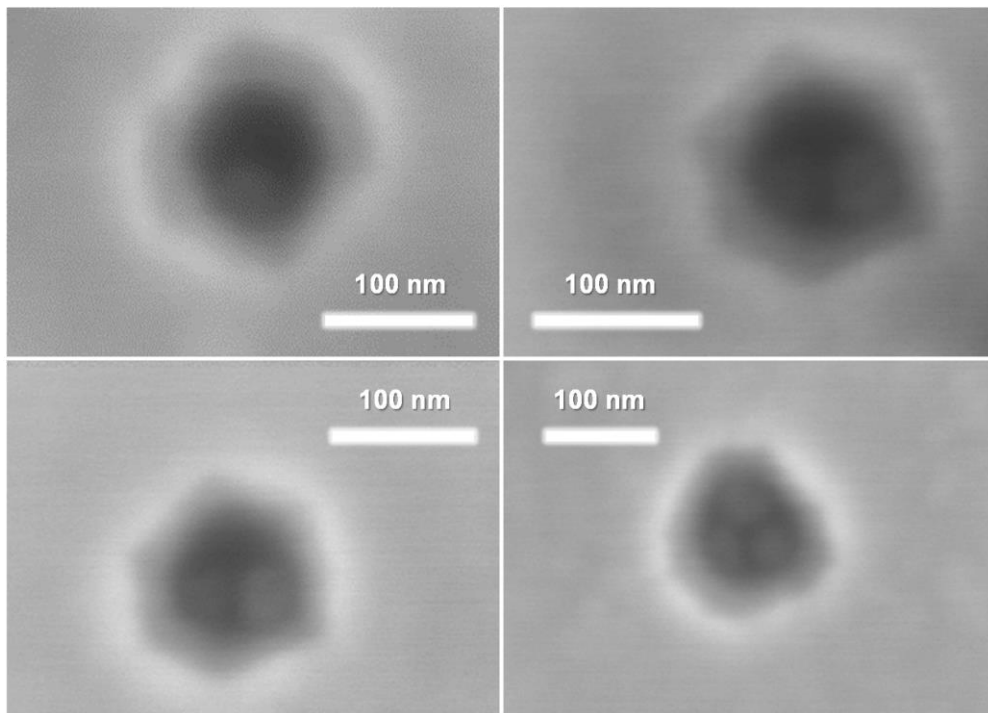


Fig. 9 Imaging of nanowells exposed briefly to avidin-coated 50 nm SiO₂ colloids binding to a biotin-functionalized membrane. The top left well has one visible colloid, the top right and bottom left two colloids each and the bottom right three colloids.

Materials

All chemicals were from SigmaAldich unless stated otherwise and ultrapure water (Milli-Q, gradient A10 system, Millipore Corporation) with resistivity 18 M Ω cm was used. All lipid vesicles consisted mainly of 1-palmitoyl-2-oleoyl-sn-glycero-3-phosphocholine (POPC, Avanti) and to this was added a small fraction of either 1,2-dihexadecanoyl-sn-glycero-3-phosphatidylethanolamine (rhodamine-DHPE, Avanti) for fluorescence experiments (1%), glycosphingolipids (histo-blood group antigen B type 1 ceramide, purified from human meconium, stored in a 2:1 mixture of chloroform and methanol) for VLP binding (5%) or 1,2-dioleoyl-sn-glycero-3-phosphoethanolamine-N-(cap biotiny) (DOPE-biotin, Avanti) for avidin binding (5%). Experiments with SiO₂ coated nanowells were performed in HEPES buffer (10 mM 4-(2-hydroxyethyl)-1-piperazineethanesulfonic acid), 50 mM NaCl, pH 7.4). Protein adsorption and fluorescence recovery was measured in PBS buffer (SigmaAldrich tablets). VLP binding which was measured in Tris buffer (10 mM tris(hydroxymethyl)-aminomethane, 100 mM NaCl, pH 7). The biotinylated copolymer was PLL(20 kDa)-g[3.5]-PEG(2 kDa)/PEG(3.4 kDa)-biotin(50%) (SuSoS AG, Switzerland). NeutrAvidin (Pierce Biotechnology) was used at a concentration of ~100 μ g/mL. Streptavidin coated silica nanoparticles (Sicastar, Micromod, Germany) with a mean diameter of 50 nm were vortexed before use (20 μ g/mL introduced).

Experimental

The nanowells were prepared colloidal lithography on Nb₂O₅, with deposition of Au and an Al₂O₃ mask followed by reactive ion etching. All details for this method have been described previously.[3] Atomic layer deposition (Savannah, Cambridge Nanotech) at a temperature of 250 °C was used to deposit a 15 nm SiO₂ layer on nanowells to be used for membrane experiments. The deposition for each cycle was about 1 nm. Silicon wafers were placed in the same chamber

along with the sensor chips and ellipsometry was performed on these wafers after deposition to confirm the thickness of deposited layer. Prior to any of the sensing experiments performed, the nanowells were cleaned by 30 min UV O₃ treatment (UVOCS) and immediately mounted into a custom made plastic flow-cell. All injections (~5 mL) were done manually (a few seconds) after which the valve was closed and binding monitored with a stagnant bulk solution (~0.5 mL). A previously described centroid algorithm was used to calculate the resonance wavelength shifts for peak and dip in the extinction spectrum.[8] The “span”, i.e. the wavelength interval defining the region used to determine the resonance wavelength, was set to the relatively low value of 50 nm for both peak and dip. A higher value can be used to provide a lower noise level but this naturally lead to more “cross talk” between the spectral resonance features and a less clear contrast between peak and dip. For 50 nm span, the short-term (timescale of seconds) noise level was ~0.005 nm for the peak and ~0.01 nm for the dip. When translating these values into a surface coverage based on a protein monolayer[8] the limit of detection is below 1 ng/cm². The baseline drift was on the order of 0.1 nm during ~1 h.

Small unilamellar vesicles for supported lipid bilayer formation were prepared by lipid film hydration followed by extrusion. The lipid mixtures in chloroform were dried onto the interior of a flask for two hours in a desiccator, after which the lipids were rehydrated in HEPES buffer, vortexed for 3 min and extruded through 100 nm and 30 nm polycarbonate membranes. The vesicle diameters were verified to be similar to those of the pores in the membrane for extrusion by nanoparticle tracking analysis (NTA, NanoSight). Bilayer formation was promoted by adding 3 mM CaCl₂ to the HEPES buffer when injecting vesicles. The system was rinsed with HEPES buffer containing 10 mM EDTA to remove Ca²⁺ afterwards.

References

- [1] Jonsson, M. P.; Jonsson, P.; Dahlin, A. B.; Hook, F., *Nano Lett* **2007**, 7 (11), 3462-3468.
- [2] Mazzotta, F.; Johnson, T. W.; Dahlin, A. B.; Shaver, J.; Oh, S.-H.; Hook, F., *ACS Photonics* **2015**, 2 (2), 256-262.
- [3] Junesch, J.; Sannomiya, T.; Dahlin, A. B., *ACS Nano* **2012**, 6 (11), 10405-10415.
- [4] Dahlin, A. B.; Mapar, M.; Xiong, K. L.; Mazzotta, F.; Hook, F.; Sannomiya, T., *Adv Opt Mater* **2014**, 2 (6), 556-564.
- [5] Sannomiya, T.; Scholder, O.; Jefimovs, K.; Hafner, C.; Dahlin, A. B., *Small* **2011**, 7 (12), 1653-1663.
- [6] Johnson, P. B.; Christy, R. W., *Phys Rev B* **1972**, 6 (12), 4370-4379.
- [7] Marie, R.; Dahlin, A. B.; Tegenfeldt, J. O.; Hook, F., *Biointerphases* **2007**, 2 (1), 49-55.
- [8] Dahlin, A. B.; Tegenfeldt J. O.; Hook F., *Anal Chem* **2006**, 78 (13), 4416-4423.